Carbon 191 (2022) 146–152

Contents lists available at ScienceDirect

Carbon

journal homepage: www.elsevier.com/locate/carbon

Narrow-chirality distributed single-walled carbon nanotube synthesized from oxide promoted Fe–SiC catalyst

Fangqian Han [a], Liu Qian [b], Qianru Wu [a], Dong Li [a], Shulan Hao [a], Lihu Feng [a], Liantao Xin [a], Tao Yang [c], Jin Zhang [b], Maoshuai He [a, *]

[a] State Key Laboratory of Eco-Chemical Engineering, Ministry of Education, Taishan Scholar Advantage and Characteristic Discipline Team of Eco-Chemical Process and Technology, College of Chemistry and Molecular Engineering, Qingdao University of Science and Technology, Qingdao, 266042, China
[b] Center for Nanochemistry, Beijing Science and Engineering Center for Nanocarbons, Beijing National Laboratory for Molecular Sciences, College of Chemistry and Molecular Engineering, Peking University, Beijing, 100871, PR China
[c] School of Environmental and Chemical Engineering, Jiangsu Ocean University, Lianyungang, 222005, Jiangsu, China

ARTICLE INFO

Article history:
Received 30 October 2021
Received in revised form
17 January 2022
Accepted 23 January 2022
Available online 25 January 2022

Keywords:
Single-walled carbon nanotubes
Fe–SiC catalyst
Catalyst promoter
Selective growth

ABSTRACT

A SiC supported iron (Fe–SiC) catalyst was developed for chemical vapor deposition (CVD) growth of carbon nanotubes. Using CO as the carbon source, sole Fe–SiC catalyst was mostly inactive for synthesizing carbon nanotubes and only trace amount of carbon deposits was produced. In contrast, the powder Fe–SiC catalyst could be activated by pressing them onto a flat SiO_2 substrate or by mixing them with porous MgO powders. Particularly, efficient growth of single-walled carbon nanotubes (SWNTs) was achieved on porous MgO promoted Fe–SiC catalyst, and predominant synthesis of (6, 5) SWNTs was realized at a reaction temperature of 650 °C. Systematic characterizations revealed that the reducibility of the Fe–SiC catalyst was enhanced by the physical contact with oxide support, which promotes the formation of small active Fe nanoparticles for the subsequent SWNT nucleation and growth. This work not only deepens our understandings to the catalyst activation mechanisms, but also helps design composite catalyst for synthesizing SWNTs.

1. Introduction

The production of single-walled carbon nanotubes (SWNTs) with a narrow chirality distribution has been a topic of increasing interest [1,2]. A catalyst template is usually required to initiate and guide the growth of an SWNT, which has been highlighted in some recent review works [3–6]. It is widely accepted that all the characteristics of the catalyst, such as the nanoparticle structure [7,8], morphology [9], and chemical composition [10,11], affect the structure and length of SWNTs, which ultimately govern the final SWNT diameter/chirality distribution. During gas phase growth processes, including floating chemical vapor deposition (CVD) [12], arc discharge [13] and laser ablation [14], randomly generated catalyst particles are mostly unfavorable for regulating the synthesized SWNTs' diameters and structures. Therefore, report on chirality-selective growth of SWNTs from free catalysts is scarce. In contrast, heterogeneous catalysts over supported materials have been extensively studied for chirality-specific growth of SWNTs by CVD [15–17]. The textural and chemical properties of the solid support are crucial for the metal dispersion and the catalyst activity. So far, the most prevalent supports adopted in catalysts include insulate magnesia (MgO) [17–20], alumina (Al_2O_3) [21], silica (SiO_2) [15,16,22] and their crystalline counterparts [23–25]. However, because of the exothermic reactions occurred on the catalyst surface during CVD process [26], the poor thermal conductivity of the oxide insulator supports could lead to the formation of local hot spots [27,28]. The accumulative reaction heat might cause the sintering of the metal catalyst, which is detrimental to the growth of SWNTs with identical diameter or chirality structure. Alternatively, SiC, which possesses high thermal conductivity, arises as a catalyst support for synthesizing carbon nanotubes [29–32]. Unfortunately, mainly multi-walled carbon nanotubes or SWNTs with poor diameter control were synthesized in the previous reports. Consequently, it is still imperative to develop an outstanding supported catalyst for chiral-selective growth of SWNTs.

In the efficient catalysts adopted for growing SWNTs, the active

* Corresponding author.
E-mail address: hemaoshuai@qust.edu.cn (M. He).

https://doi.org/10.1016/j.carbon.2022.01.052
0008-6223/

metal components are mainly Fe, Co and Ni [2,33]. Among them, Fe-based catalyst is extensively investigated because of its low cost and large carbon solubility [34,35], which facilitates the growth of small diameter SWNTs by a perpendicular mode [36]. Nevertheless, the strong interactions between the Fe phase and the oxide support makes the reduction of small iron oxide nanoparticles difficult [37,38], causing a low number of active Fe nanoparticles available for carbon nanotube synthesis at a low reaction temperature. Indeed, it was previously demonstrated that only a trace amount of multi-walled carbon nanotubes could be generated at 600 °C on an MgO supported Fe catalyst [17]. The result is correlated with the H_2-temperature programmed reduction (TPR) profile of MgO supported iron oxide catalyst, which exhibits a complete reduction at a temperature higher than 700 °C [38]. To improve the reduction of supported Fe nanoparticles, a promoter metal, like Ru [16] or Pt [39], was usually introduced to enhance their reduction. However, the presence of a 2nd metal might complicate the post-growth purification process. Moreover, the use of expensive noble metal limits the wide application in catalytically growing SWNTs. As a result, a cost-efficient promoter is preferred for enhancing the chirality-selective growth of SWNTs.

In the work, we developed a SiC supported Fe catalyst (Fe–SiC) for CVD growth of carbon nanotubes. Although the Fe–SiC catalyst alone is inactive for growing carbon nanotubes, it can be activated by physical contact with either flat SiO_2 substrate or porous MgO powders. On one hand, the use of SiC as catalyst support avoids the formation of local hot spots on the support surface; On the other hand, the oxide promoter enhances the reduction of iron oxide, facilitating the formation of small, active Fe nanoparticles for growing SWNTs. Consequently, predominant (6, 5) SWNT growth was achieved on the MgO promoted Fe–SiC catalyst at 650 °C. This work evidences the application of SiC supported catalyst for growing SWNTs with a high chirality selectivity.

2. Experiments

2.1. Preparation of Fe–SiC catalyst

The Fe–SiC catalyst was prepared by an impregnation method. Firstly, $Fe(NO_3)_3 \cdot 9H_2O$ (Aladdin, 99.99%) with a mass of 0.25 g was dissolved in 50 ml H_2O. After mixing with 5.0 g SiC (Macklin, 99.9%), the impregnated catalyst was dried overnight and ground into fine powders. Finally, air calcination was performed in a muffle furnace at 600 °C for 4 h.

2.2. CVD growth of carbon nanotubes

A horizontal reactor with a quartz tube (inner diameter: 40 mm) was applied for CVD growth of carbon nanotubes. After loading Fe–SiC powders inside the reactor center, the reactor was flushed with 300 sccm Ar and heated to desired temperatures. CO with a flow rate of 300 sccm was subsequently introduced to the CVD reactor to replace Ar and the reaction lasted 35 min. The system was finally cooled to room temperature with 300 sccm Ar.

There are two strategies to promote the growth of SWNTs. One is to press the Fe–SiC powders onto bare SiO_2/Si substrate with an oxide layer thickness of 300 nm. The other is to mix Fe–SiC catalyst with porous MgO by grinding them together (the weight ratio between Fe–SiC to MgO is ~1:2). Noted that the porous MgO was prepared by thermal decomposition of magnesium carbonate hydroxide.

2.3. Characterizations of catalysts

The crystal structures of raw SiC support and Fe–SiC catalysts were characterized by X-ray diffraction (XRD, Bruker D8 advance) with a Cu K_a ($\lambda = 0.15406$ nm) radiation in the scanning angle range of 20°-90°. X-ray photoelectron spectroscopy (XPS, Thermo Fisher ESCALAB 250 Xi) was carried out to examine the SiC support and catalyst chemical states. Photoelectrons with 1486.6 eV energy were excited by an Al Kα X-ray source. The morphologies of the support and catalyst were investigated by transmission electron microscopy (TEM, JEOL JEM-2100PLUS). The element distributions of catalyst were characterized by energy-dispersive X-ray spectroscopy (EDS, X-MaxN 80T) elemental mapping. H_2-temperature programed reduction (H_2-TPR) was conducted in a AutoChem 2920 system equipped with a thermal conductivity detector (TCD). During the TPR process, the sample temperature was increased to 900 °C at a rate of 10 °C/min.

2.4. Characterizations of carbon nanotubes

The as-synthesized carbon nanotubes were examined by Raman spectroscopy (Renishaw, inVia). Spectra were collected over many random spots on each sample with 633 nm and 532 nm excitation lasers. The morphology of carbon nanotubes was characterized by scanning electron microscopy (SEM HITACHI, regulus8100) and TEM. For carbon nanotubes synthesized on MgO promoted Fe–SiC catalyst, the powder MgO was removed by acid hydrochloric (HCl) and the residual materials were characterized by thermogravimetric analysis (TGA, Netzsch TG-209F3). HCl-purified carbon nanotubes were dispersed in an aqueous solution of sodium deoxycholate (SDC, 2 wt%) by sonication. After centrifugation at 100,000 g for 50 min, the decanted supernatant was subjected to ultraviolet–visible–near-infrared (UV–vis–NIR, Agilent Cary 5000) absorption and photoluminescence (PL, HORIBA Jobin Yvon, Fluorolog-3) spectroscopy characterizations. To measure the SWNT diameter, the decanted supernatant was dispersed on (3-aminopropyl) triethoxysilane (APTES, Macklin, 99%)-coated SiO_2/Si substrate and subjected to atomic force microscopy (AFM, MultiMode 8-HR) characterizations.

3. Results and discussion

SiC is one of the most remarkable catalyst supports because of its intrinsic physicochemical properties (ESI Fig. S1), such as good chemical inertness and high thermal conductivity, which avoids the formation of local hot spots on the support surface during reaction process, beneficial to uniform SWNT growth. Fig. 1a displays the XRD pattern of the prepared Fe–SiC powers, where two sets of diffraction peaks were detected, and all the 2θ peaks arise from SiC phase (JCPDS card No.: 29-1131, 49-1428). The lack of iron oxide features in the XRD profile indicates the well dispersion of Fe-containing components. The presence of Fe in the catalyst is verified by the Fe 2p XPS spectrum (Fig. 1b). The binding energies correspond with those of iron oxide phases. Meanwhile, the presence of satellite structure between the Fe 2p doublet at 8.0 eV higher than the binding energy of Fe $2p_{3/2}$ is unique for α-Fe_2O_3 [40]. Although the heat conductivity of SiC is much higher than that of oxide insulator support [41,42] SiC support is unfavorable for stabilizing metal particles because of its chemical inertness. Therefore, when using SiC as support in heterogeneous catalysis, a thin oxide layer is generally coated on the SiC surface to stabilize the dispersed metal particles [42–45]. For example, Liu et al. [43] prepared a TiO_2-decorated SiC for enhancing the Co catalyst properties for Fischer-Tropsch synthesis. The nanoscale introduction of the TiO_2 promotes the formation of small Co nanoparticles due to the suitable metal-support interaction. Besides, a straightforward strategy for anchoring metal nanoparticles on SiC surface is to perform air calcination, which leads to the formation of a

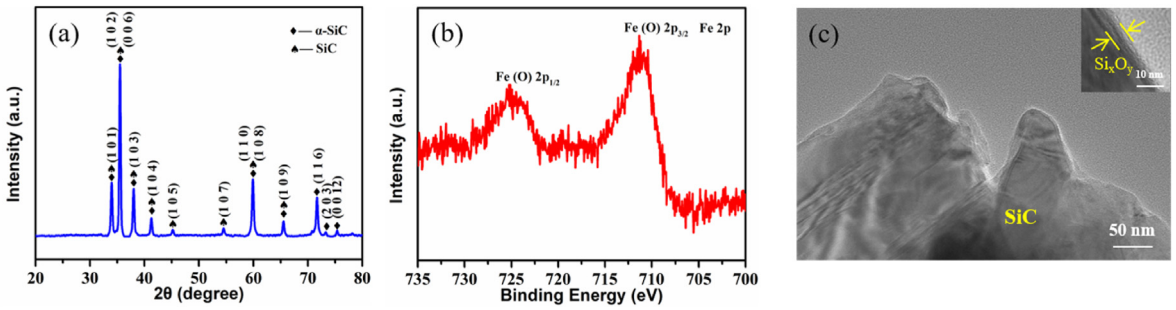

Fig. 1. (a) XRD pattern of the Fe–SiC catalyst. (b) XPS spectrum of Fe 2p in the Fe–SiC catalyst. (c) TEM image of Fe–SiC catalyst (Inset is a magnified image).

homogeneous Si_xO_y layer [45]. In agreement with previous findings, a thin amorphous layer was also observed on the surface of SiC support after air calcination of the Fe–SiC catalyst (Fig. 1c). By comparing with the TEM image of raw SiC (ESI Fig. S1d), it can be concluded that the Si_xO_y layer is formed during the Fe–SiC catalyst calcination process.

Growth of carbon nanotubes was initially carried out at 850 °C using CO CVD. ESI Fig. S2 presents the Raman spectrum of the product grown on the Fe–SiC catalyst. The lack of radial breathing mode (RBM) and the relative high D mode intensity indicate that the products could be multi-walled carbon nanotubes or carbon fibers. The results are in agreement with the report by Shahi et al. [31], who investigated the effect of catalyst combination ratio on carbon nanotube growth over Fe–Co/SiC catalyst and found that only multi-walled carbon nanotube was generated no matter what the metal combination ratio was.

During CVD process, the catalyst activity could be influenced by the nature of the catalyst support, the metal dispersion and the preparation method. Even after nearly 30 years of research on developing catalysts for growing SWNTs, it continues to be a challenge to unravel the catalyst activation mechanisms [3,26]. Although the nature of the active catalyst and the dynamic nature of metal-carbon system under reaction environments complicate any interpretation on catalyst performance, the reduction of catalyst seems to be of great importance in activating metal oxide catalyst [46]. Too easy reduction of metal oxide causes the sintering of metal particles, accounting for the formation of large diameter multi-walled carbon nanotubes or catalyst deactivation. In the case of Fe–SiC catalyst, FeO_x is difficult to reduce (ESI Fig. S3) because of the Si_xO_y layer covering, which induces a strong catalyst-support interactions between Fe species and insulator oxides.

With the aim of promoting the activation of Fe–SiC catalyst, a "pressing on oxide" method was adopted [21]. Fig. 2a shows an SEM image of carbon nanotubes grown at 850 °C by pressing the Fe–SiC catalyst on a flat SiO_2/Si substrate. Clearly, carbon nanotubes are observed to protrude out of the interfaces between the powder Fe–SiC and SiO_2/Si. Raman characterizations confirmed the growth of SWNTs and the detected RBMs acquired with two laser wavelengths were summarized in Fig. 2b and ESI Fig. S4a. Most RBMs are located in the frequency range of 180–200 cm^{-1}, corresponding to SWNTs with diameters close to 1.2 nm. The activation of the Fe–SiC catalyst is attributed to the presence of O atoms on the SiO_2/Si surface, which help dissociate the CO molecules to generate active carbon atoms [21,47]. The dissociated carbon atoms could diffuse to the adjacent Fe–SiC, promoting the reduction of iron oxide for growing SWNTs. Such a catalyst activity enhancement could be further strengthened by mixing the Fe–SiC power with porous MgO, which could donate electrons to the anti-bond orbitals of absorbed CO molecules, thus enhancing the dissociation of CO [48]. Fig. 2c and ESI Fig. S4b show the Raman spectra of the products grown from the MgO promoted Fe–SiC catalyst at 850 °C. The RBM frequencies are similar to those acquired from individual SWNTs on flat substrate (Fig. 2b, ESI Fig. S4a). The generation of SWNTs at lower reaction temperatures was also verified by SEM and TEM characterizations (ESI Fig. S5). The results verify that porous MgO could also enhance the growth of SWNTs, thus making the bulk synthesis of SWNTs possible.

TEM was performed to characterize the MgO promoted Fe–SiC catalyst (Fig. 3a). Fig. 3b-g presents the elemental mapping of the catalyst and the overlapped image. Clearly, all the elements, such as Mg, Si, C, O and Fe, are well dispersed and overlapped, indicating that the porous MgO are contacted well with the Fe–SiC catalyst, thus promoting the growth of SWNTs during CVD process. Fig. 4a shows the H_2-TPR profile of the porous MgO promoted Fe–SiC catalyst. Compared with raw Fe–SiC catalyst (ESI Fig. S3), the promoted catalyst is easier to reduce. Three distinct reduction peaks, centered at 430 °C, 526 °C and 588 °C, are respectively assigned as the gradual reduction of Fe_2O_3 to Fe_3O_4, Fe_3O_4 to FeO and FeO to metallic Fe. Although the active phase of Fe for growing carbon nanotubes could be Fe_3C or Fe_2C_5 [8,39], the reduction to metallic

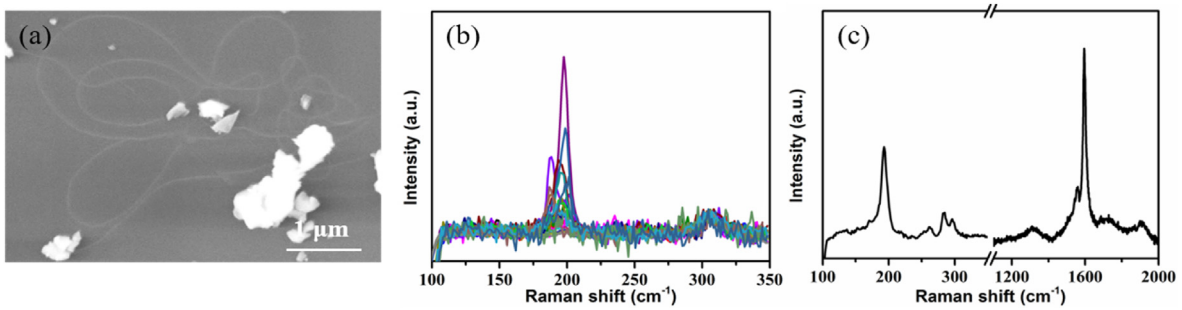

Fig. 2. (a) SEM image of carbon nanotubes grown from Fe–SiC catalyst pressed on flat SiO_2/Si substrate at 850 °C. (b) RBMs acquired from SWNTs grown from Fe–SiC catalyst pressed on flat SiO_2/Si substrate at 850 °C. (c) Raman spectrum of SWNTs grown on MgO promoted Fe–SiC catalyst at 850 °C by CO CVD. The excitation wavelength is 633 nm.

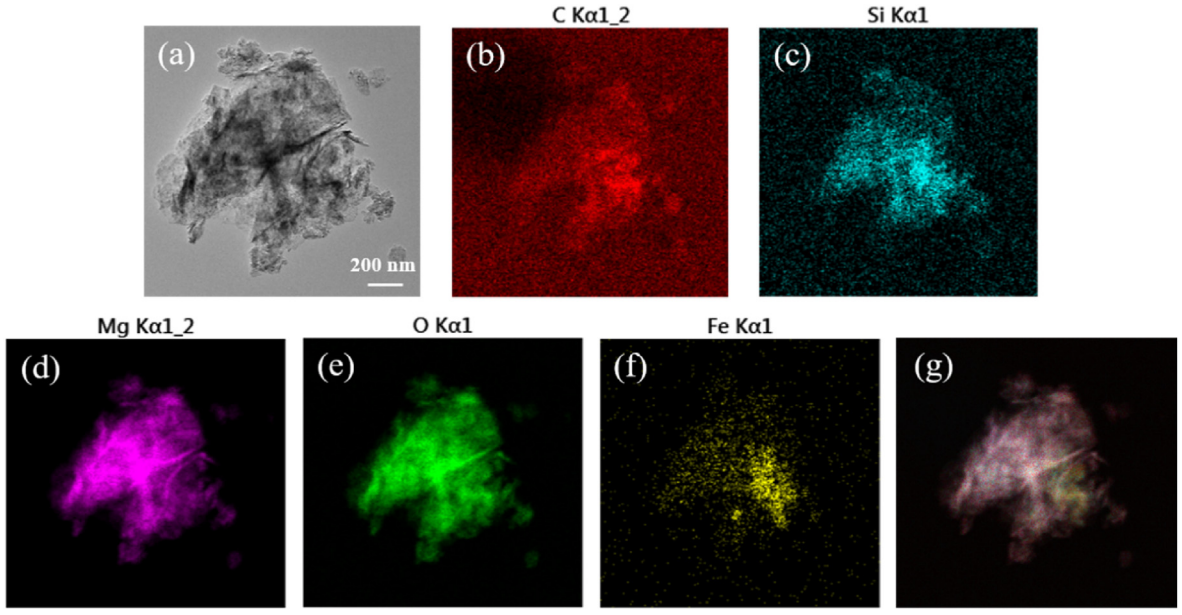

Fig. 3. (a) TEM image of MgO promoted Fe–SiC catalyst. (b) C (c) Si (d) Mg (e) O and (f) Fe EDS elemental maps of the MgO promoted Fe–SiC catalyst. (g) Overlapped image of catalyst.

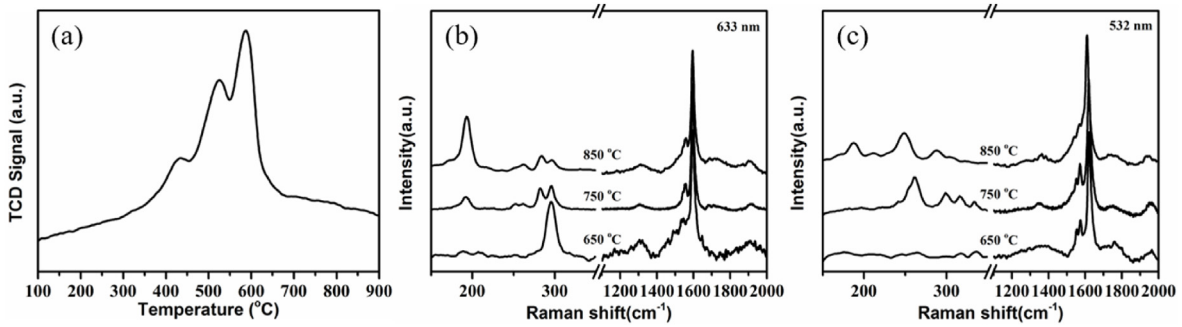

Fig. 4. (a) H_2-TPR profile of MgO promoted Fe–SiC catalyst. (b) (c) Raman spectra of SWNTs grown at different temperatures with 633 nm and 532 nm lasers respectively.

phase is a prerequisite for the subsequent carburization. Fig. 4b and c presents the Raman spectra of carbon nanotubes grown at different temperatures. With increasing reaction temperature, the diameters of the SWNTs increase. The phenomenon is in agreement with many previous findings [15–17]. Several reasons could be responsible for the temperature dependence of SWNT diameter evolution. First is the particle sintering or coalescence caused by elevated temperature. At high reaction temperatures, Ostwald ripening becomes severe, leading to the generation of large diameter catalyst particles for large diameter SWNT growth. Second, a high CVD temperature provides sufficient energy to overcome the nucleation barriers of different SWNT species [49], causing the diversity of SWNT structures. Third is related to the entropy-driven stability of SWNTs [50]. The stability of a (n, m) chiral SWNT depends on the interfacial energy of armchair and zigzag contacts on catalyst surface, the difference of which becomes smaller at high temperatures, resulting in a broad chirality distribution. Consequently, low temperature growth is highly preferred for synthesizing SWNTs with a narrow chirality distribution.

The chirality distribution of SWNTs was investigated by absorption spectroscopy. Fig. 5a compares the absorption spectra of SWNTs grown at 750 °C and 650 °C. In agreement with Raman characterizations, SWNTs grown at 750 °C exhibit a broad chirality distribution. Near-armchair species, including (6, 5), (7, 5), (7, 6), (8, 6) and (8, 7) tubes, are the main products. The preferential synthesis of (n, n-1) nanotubes can be explained by the nucleation of (n, n) tubes and their structural change by kinetically incorporating an energetically preferred pentagon-heptagon pair in the tube wall [51]. Generally, the active catalyst surface adopts a flat low-index plane, like (111) plane with a 3-fold symmetry. According to the symmetry match concept [23], SWNTs with similar symmetry, like (6, 6) ones, are thermodynamically stable when nucleated on the catalyst surface. However, the perfect match between the (6, 6) SWNT and the underlying catalyst makes the incorporation of new carbon atoms to the tube rims extremely difficult [27], and the SWNT growth rate is very slow. Under near-equilibrium growth conditions, a possible chirality mutation could change (n, n) SWNTs into (n, n-1), (n+1, n), (n+1, n-1), (n+2, n) species [51]. The near-armchair tubes have kink sites at the edge for carbon insertion, and thus possess reasonable SWNT growth rates and lengths. Decreasing reaction temperature favors the synthesis of small diameter SWNTs with a narrow chirality distribution. For example, SWNTs grown at 650 °C exhibit an enrichment of (6, 5) species (Fig. 5a). The preferential (6, 5) nanotube synthesis was also confirmed by PL map of the SWNT dispersion (Fig. 5b). Fig. 5c presents the PL intensity ratios between the (6, 5) SWNT and the (7,

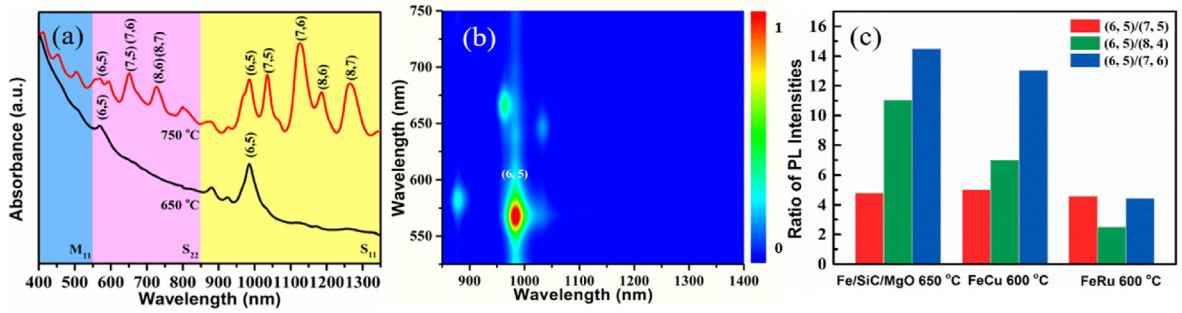

Fig. 5. (a) UV–vis–NIR absorption spectra of SDC-dispersed SWNTs grown at 650 °C and 750 °C. The label S_{11} (yellow) and S_{22} (pink) correspond to the first and the second van Hove singularities of the semiconducting SWNTs; the M_{11} (blue) corresponds to the overlapping absorption bands of the first van Hove singularities from metallic SWNTs. (b) PL contour plots as a function of excitation and emission energies of SDC-dispersed SWNTs grown at 650 °C. (c) PL intensity ratios between the (6, 5) SWNT and the (7, 5), (8, 4), and (7, 6) tubes in 650 °C grown form MgO-promoted Fe–SiC catalyst versus solid supported FeCu catalyst [17] and FeRu catalyst [16].

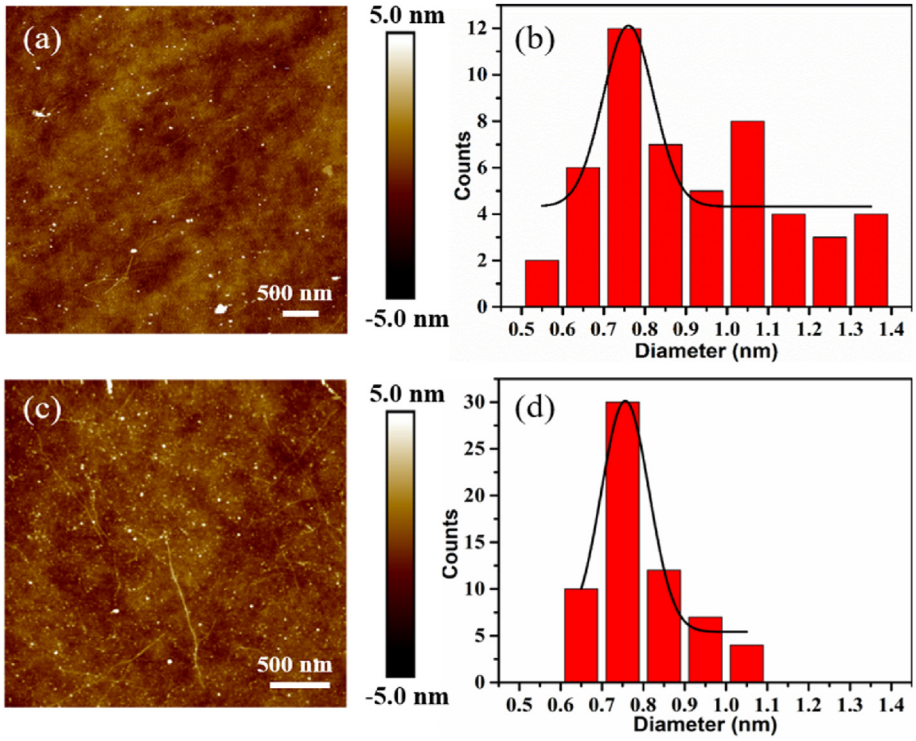

Fig. 6. (a) AFM image and (b) Diameter distributions of the SWNTs grown at 750 °C. (c) AFM image and (d) Diameter distributions of the SWNTs grown at 650 °C.

5), (8, 4) and (7, 6) tubes. Compared with FeCu catalyst [17] and FeRu catalyst [16] which are highly selective to the (6, 5) tube, Fe–SiC catalyst promoted by porous MgO has much higher PL intensity ratios, indicating that it is more enriched with the (6, 5) tube. The narrow SWNT chirality distribution could be correlated with the high thermal conductivity of SiC support, which avoid the formation of hot spots on the catalyst surface. In addition, the use of Fe as the active component and CO as the carbon precursor promotes the growth of SWNTs with a perpendicular mode [34].

With the aim to estimate the yield and purity of the products, TGA was carried out on the products synthesized at 650 °C after rinsing with HCl (ESI Fig. S6). The TGA profile exhibits a primary oxidation temperature of 550 °C, which is higher than other previously reported SWNTs with similar diameter distribution [52,53], further highlighting the advantages of the oxide-promoted growth method. Besides, AFM was applied to characterize the produced SWNTs. Grounded on the height measurement, the diameter distributions of the SWNTs synthesized at different temperature were deduced. Fig. 6a and b displays the typical AFM images and diameters of the dispersed SWNTs synthesized from the MgO promoted Fe–SiC catalyst at 750 °C, exhibiting an average diameter of 0.92 nm. In agreement with optical characterization results, decreasing reaction temperature leads to the generation of SWNTs with smaller diameters (Fig. 6c and d). The average diameter of 650 °C grown SWNTs is 0.79 nm, close to the diameter of (6, 5) tube. Meanwhile, it is noted that many previous works [18,37,54,55] demonstrate that the diameter and chirality distributions of SWNTs deduced by different techniques generally do not show striking differences.

4. Conclusions

In summary, a SiC supported Fe catalyst was applied for the synthesis of carbon nanotubes. By physically mixing the catalyst with oxide support, the reduction of the Fe–SiC catalyst was enhanced, promoting the growth of SWNTs at relatively low

temperatures. The temperature effect on the diameters of SWNTs synthesized from porous MgO promoted Fe–SiC catalyst was investigated and predominant (6, 5) SWNT growth was achieved at a temperature of 650 °C. This work not only highlights the importance of oxide support in activating catalyst particles, but also guide the development of oxide promoted heterogeneous catalysts for chiral selective synthesis of SWNTs.

CRediT authorship contribution statement

Fangqian Han: Conceptualization, Investigation, Formal analysis, Writing – original draft. **Liu Qian:** Investigation, Writing – review & editing. **Qianru Wu:** Investigation, Writing – review & editing. **Dong Li:** Investigation, Validation, Data curation, Writing – review & editing. **Shulan Hao:** Visualization, Resources. **Lihu Feng:** Investigation, Resources. **Liantao Xin:** Investigation, Resources. **Tao Yang:** Methodology, Investigation. **Jin Zhang:** Methodology, Investigation. **Maoshuai He:** Conceptualization, Data curation, Writing – original draft, Writing – review & editing, Supervision.

Declaration of competing interest

The authors declare that they have no known competing financial interests or personal relationships that could have appeared to influence the work reported in this paper.

Acknowledgements

The authors would like to acknowledge the National Natural Science Foundation of China (51972184) and Key Basic Research Project of Shandong Province (ZR2019ZD49). Funding from Taishan Scholar Advantage and Characteristic Discipline Team of Eco Chemical Process and Technology is also acknowledged. Prof. Z. Li is acknowledged for the experimental support.

Appendix A. Supplementary data

Supplementary data to this article can be found online at https://doi.org/10.1016/j.carbon.2022.01.052.

References

[1] M. He, S. Zhang, Q. Wu, H. Xue, D. Wang, J. Zhang, et al., Designing catalysts for chirality-selective synthesis of single-walled carbon nanotubes: past success and future opportunity, Adv. Mater. 31 (2019) 1800805.
[2] H. Wang, Y. Yuan, L. Wei, K. Goh, D. Yu, Y. Chen, Catalysts for chirality selective synthesis of single-walled carbon nanotubes, Carbon 81 (2015) 1–19.
[3] M. He, S. Zhang, J. Zhang, Horizontal single-walled carbon nanotube arrays: controlled synthesis, characterizations, and applications, Chem. Rev. 120 (2020) 12592–12684.
[4] R. Zhang, Y. Zhang, F. Wei, Horizontally aligned carbon nanotube arrays: growth mechanism, controlled synthesis, characterization, properties and applications, Chem. Soc. Rev. 46 (2017) 3661–3715.
[5] F. Yang, M. Wang, D. Zhang, J. Yang, M. Zheng, Y. Li, Chirality pure carbon nanotubes: growth, sorting, and characterization, Chem. Rev. 120 (2020) 2693–2758.
[6] X. Wang, M. He, F. Ding, Chirality-controlled synthesis of single-walled carbon nanotubes-from mechanistic studies toward experimental realization, Mater. Today 21 (2018) 845–860.
[7] S. Mazzucco, Y. Wang, M. Tanase, M. Picher, K. Li, Z.J. Wu, et al., Direct evidence of active and inactive phases of Fe catalyst nanoparticles for carbon nanotube formation, J. Catal. 319 (2014) 54–60.
[8] C.T. Wirth, B.C. Bayer, A.D. Gamalski, S. Esconjauregui, R.S. Weatherup, C. Ducati, et al., The phase of iron catalyst nanoparticles during carbon nanotube growth, Chem. Mater. 24 (2012) 4633–4640.
[9] M. He, H. Amara, H. Jiang, J. Hassinen, C. Bichara, R.H. Ras, et al., Key roles of carbon solubility in single-walled carbon nanotube nucleation and growth, Nanoscale 7 (2015) 20284–20289.
[10] W.-H. Chiang, R. Mohan Sankaran, Linking catalyst composition to chirality distributions of as-grown single-walled carbon nanotubes by tuning Ni_xFe_{1-x} nanoparticles, Nat. Mater. 8 (2009) 882–886.
[11] O.V. Yazyev, A. Pasquarello, Effect of metal elements in catalytic growth of carbon nanotubes, Phys. Rev. Lett. 100 (2008) 156102.
[12] P. Nikolaev, Gas-phase production of single-walled carbon nanotubes from carbon monoxide: a review of the HiPco process, J. Nanosci. Nanotechnol. 4 (2004) 307–316.
[13] N. Arora, N. Sharma, Arc discharge synthesis of carbon nanotubes: comprehensive review, Diam. Relat. Mater. 50 (2014) 135–150.
[14] Y. Zhang, H. Gu, S. Iijima, Single-wall carbon nanotubes synthesized by laser ablation in a nitrogen atmosphere, Appl. Phys. Lett. 73 (1998) 3827–3829.
[15] S.M. Bachilo, L. Balzano, J.E. Herrera, F. Pompeo, D.E. Resasco, R.B. Weisman, Narrow (n,m)-distribution of single-walled carbon nanotubes grown using a solid supported catalyst, J. Am. Chem. Soc. 125 (2003) 11186–11187.
[16] X. Li, X. Tu, S. Zaric, K. Welsher, W.S. Seo, W. Zhao, et al., Selective synthesis combined with chemical separation of single-walled carbon nanotubes for chirality selection, J. Am. Chem. Soc. 129 (2007) 15770–15771.
[17] M. He, A.I. Chernov, P.V. Fedotov, E.D. Obraztsova, J. Sainio, E. Rikkinen, et al., Predominant (6, 5) single-walled carbon nanotube growth on a copper-promoted iron catalyst, J. Am. Chem. Soc. 132 (2010) 13994–13996.
[18] M. He, H. Jiang, B. Liu, P.V. Fedotov, A.I. Chernov, E.D. Obraztsova, et al., Chiral-selective growth of single-walled carbon nanotubes on lattice-mismatched epitaxial cobalt nanoparticles, Sci. Rep. 3 (2013) 1460.
[19] M. He, D. Li, T. Yang, D. Shang, A.I. Chernov, P.V. Fedotov, et al., A robust $Co_xMg_{1-x}O$ catalyst for predominantly growing (6, 5) single-walled carbon nanotubes, Carbon 153 (2019) 389–395.
[20] M. He, X. Wang, L. Zhang, Q. Wu, X. Song, A.I. Chernov, et al., Anchoring effect of Ni^{2+} in stabilizing reduced metallic particles for growing single-walled carbon nanotubes, Carbon 128 (2018) 249–256.
[21] Q. Wu, H. Zhang, C. Ma, D. Li, L. Xin, M. He, et al., SiO_2-promoted growth of single-walled carbon nanotubes on an alumina supported catalyst, Carbon 176 (2021) 367–373.
[22] H. Wang, B. Wang, X.Y. Quek, L. Wei, J.W. Zhao, L.J. Li, et al., Selective synthesis of (9, 8) single walled carbon nanotubes on cobalt incorporated TUD-1 catalysts, J. Am. Chem. Soc. 132 (2010) 16747–16749.
[23] S. Zhang, L. Kang, X. Wang, L. Tong, L. Yang, Z. Wang, et al., Arrays of horizontal carbon nanotubes of controlled chirality grown using designed catalysts, Nature 543 (2017) 234–238.
[24] D. Yuan, L. Ding, H. Chu, Y. Feng, T.P. McNicholas, J. Liu, Horizontally aligned single-walled carbon nanotube on quartz from a large variety of metal catalysts, Nano Lett. 8 (2008) 2576–2579.
[25] M. Maret, K. Hostache, M. Schouler, B. Marcus, F. Rousseldherbey, M. Albrecht, et al., Oriented growth of single-walled carbon nanotubes on a MgO(001) surface, Carbon 45 (2007) 180–187.
[26] V. Jourdain, C. Bichara, Current understanding of the growth of carbon nanotubes in catalytic chemical vapour deposition, Carbon 58 (2013) 2–39.
[27] M. Lacroix, L. Dreibine, B. de Tymowski, F. Vigneron, D. Edouard, D. Bégin, et al., Silicon carbide foam composite containing cobalt as a highly selective and re-useable fischer-tropsch synthesis catalyst, Appl. Catal., A 397 (2011) 62–72.
[28] P. Nguyen, C. Pham, Innovative porous SiC-based materials: from nanoscopic understandings to tunable carriers serving catalytic needs, Appl. Catal., A 391 (2011) 443–454.
[29] A. Cao, V.P. Veedu, X. Li, Z. Yao, M.N. Ghasemi-Nejhad, P.M. Ajayan, Multi-functional brushes made from carbon nanotubes, Nat. Mater. 4 (2005) 540–545.
[30] L. Ci, J. Bai, Novel micro/nanoscale hybrid reinforcement: multiwalled carbon nanotubes on SiC particles, Adv. Mater. 16 (2004) 2021–2024.
[31] F. Shahi, M. Akbarzadeh Pasha, The effect of catalyst combination ratioon growth of carbon nanotubesover Fe-Co/nanometric SiC by chemical vapor deposition, Sci. Iran. 23 (2016) 1517–1523.
[32] T. Murakami, T. Sako, H. Harima, K. Kisoda, K. Mitikami, T. Isshiki, Raman study of SWNTs grown by CCVD method on SiC, Thin Solid Films 464 (2004) 319–322.
[33] M. He, X. Wang, S. Zhang, H. Jiang, F. Cavalca, H. Cui, et al., Growth kinetics of single-walled carbon nanotubes with a (2n,n) chirality selection, Sci. Adv. 5 (2019) eaav9668.
[34] M. He, Y. Magnin, H. Amara, H. Jiang, H. Cui, F. Fossard, et al., Linking growth mode to lengths of single-walled carbon nanotubes, Carbon 113 (2017) 231–236.
[35] A. Moisala, A.G. Nasibulin, E.I. Kauppinen, The role of metal nanoparticles in the catalytic production of single-walled carbon nanotubes-a review, J. Phys. Condens. Matter 15 (2003). S3011.
[36] M. He, Y. Wang, X. Zhang, H. Zhang, Y. Meng, D. Shang, et al., Stability of iron-containing nanoparticles for selectively growing single-walled carbon nanotubes, Carbon 158 (2020) 795–801.
[37] M. He, B. Liu, A.I. Chernov, E.D. Obraztsova, I. Kauppi, H. Jiang, et al., Growth mechanism of single-walled carbon nanotubes on iron-copper catalyst and chirality studies by electron diffraction, Chem. Mater. 24 (2012) 1796–1801.
[38] A.E. Awadallah, M.S. Abdel-Mottaleb, A.A. Aboul-Enein, M.M. Yonis, A.K. Aboul-Gheit, Catalytic decomposition of natural gas to CO/CO_2-free hydrogen production and carbon nanomaterials using MgO-supported monometallic iron family catalysts, Chem. Eng. Commun. 202 (2015) 163–174.
[39] M. He, H. Jin, L. Zhang, H. Jiang, T. Yang, H. Cui, et al., Environmental transmission electron microscopy investigations of Pt-Fe_2O_3 nanoparticles for nucleating carbon nanotubes, Carbon 110 (2016) 243–248.
[40] D.D. Hawn, B.M. DeKoven, Deconvolution as a correction for photoelectron

inelastic energy losses in the core level XPS spectra of iron oxides, Surf. Interface Anal. 10 (1987) 63–74.
[41] J. Sun, Q. Feng, Q. Liu, S. Ji, Y. Fang, X. Peng, et al., An Al_2O_3-coated SiC-supported Ni catalyst with enhanced activity and improved stability for production of synthetic natural gas, Ind. Eng. Chem. Res. 57 (2018) 14899–14909.
[42] R. Moene, M. Makkee, J. Moulijn, High surface area silicon carbide as catalyst support characterization and stability, Appl. Catal., A 167 (1998) 321–330.
[43] Y. Liu, B. de Tymowski, F. Vigneron, I. Florea, O. Ersen, C. Meny, et al., Titania-decorated silicon carbide-containing cobalt catalyst for fischer-tropsch synthesis, ACS Catal. 3 (2013) 393–404.
[44] Y. Liu, I. Florea, O. Ersen, C. Pham-Huu, C. Meny, Silicon carbide coated with TiO_2 with enhanced cobalt active phase dispersion for fischer-tropsch synthesis, Chem. Commun. 51 (2015) 145–148.
[45] D. Wang, C. Chen, J. Wang, L. Jia, B. Hou, D. Li, Silicon carbide supported cobalt for fischer-tropsch synthesis: probing into the cause of the intrinsic excellent catalytic performance, RSC Adv. 5 (2015) 98900–98903.
[46] M. He, A.I. Chernov, P.V. Fedotov, E.D. Obraztsova, E. Rikkinen, Z. Zhu, et al., Selective growth of SWNTs on partially reduced monometallic cobalt catalyst, Chem. Commun. 47 (2011) 1219–1221.
[47] X. Xu, Z. Zhang, L. Qiu, J. Zhuang, L. Zhang, H. Wang, et al., Ultrafast growth of single-crystal graphene assisted by a continuous oxygen supply, Nat. Nanotechnol. 11 (2016) 930.
[48] L. Chen, X. Tian, Y. Fu, J. Shen, The effect of surface acidic and basic properties of highly loaded Co catalysts on the fischer-tropsch synthesis, Catal. Commun. 28 (2012) 155–158.
[49] V.I. Artyukhov, E.S. Penev, B.I. Yakobson, Why nanotubes grow chiral? Nat. Commun. 5 (2014) 4892.
[50] Y. Magnin, H. Amara, F. Ducastelle, A. Loiseau, C. Bichara, Entropy-driven stability of chiral single-walled carbon nanotubes, Science 362 (2018) 212–215.
[51] S. Zhang, X. Wang, F. Yao, M. He, D. Lin, H. Ma, et al., Controllable growth of (n, n-1) family of semiconducting carbon nanotubes, Chemistry 5 (2019) 1182–1193.
[52] H.N. Yehia, R.K. Draper, C. Mikoryak, E.K. Walker, P. Bajaj, I.H. Musselman, et al., Single-walled carbon nanotube interactions with HeLa cells, J. Nanobiotechnol. 5 (2007) 1–17.
[53] Q. Wu, L. Qiu, L. Zhang, H. Liu, C. Ma, M. He, et al., Temperature-dependent selective nucleation of single-walled carbon nanotubes from stabilized catalyst nanoparticles, Chem. Eng. J. (2021), 133487.
[54] A. Castan, S. Forel, F. Fossard, J. Defillet, A. Ghedjatti, D. Levshov, et al., Assessing the reliability of the Raman peak counting method for the characterization of SWCNT diameter distributions: a cross characterization with TEM, Carbon 171 (2021) 968–979.
[55] Y. Tian, H. Jiang, J.V. Pfaler, Z. Zhu, A.G. Nasibulin, T. Nikitin, et al., Analysis of the size distribution of single-walled carbon nanotubes using optical absorption spectroscopy, J. Phys. Chem. Lett. 1 (2010) 1143–1148.